Electronic Supplementary Information

Quantum Interference and Spin Filtering Effects in Photo-responsive Single Molecular Device

Ashima Bajaj, Rishu Khurana, and Md. Ehesan Ali*

Institute of Nano Science and Technology, Sector-81, Mohali-140306, Punjab, India

E-mail: ehesan.ali@inst.ac.in

Contents

1 Molecular orbital energies of isolated molecules

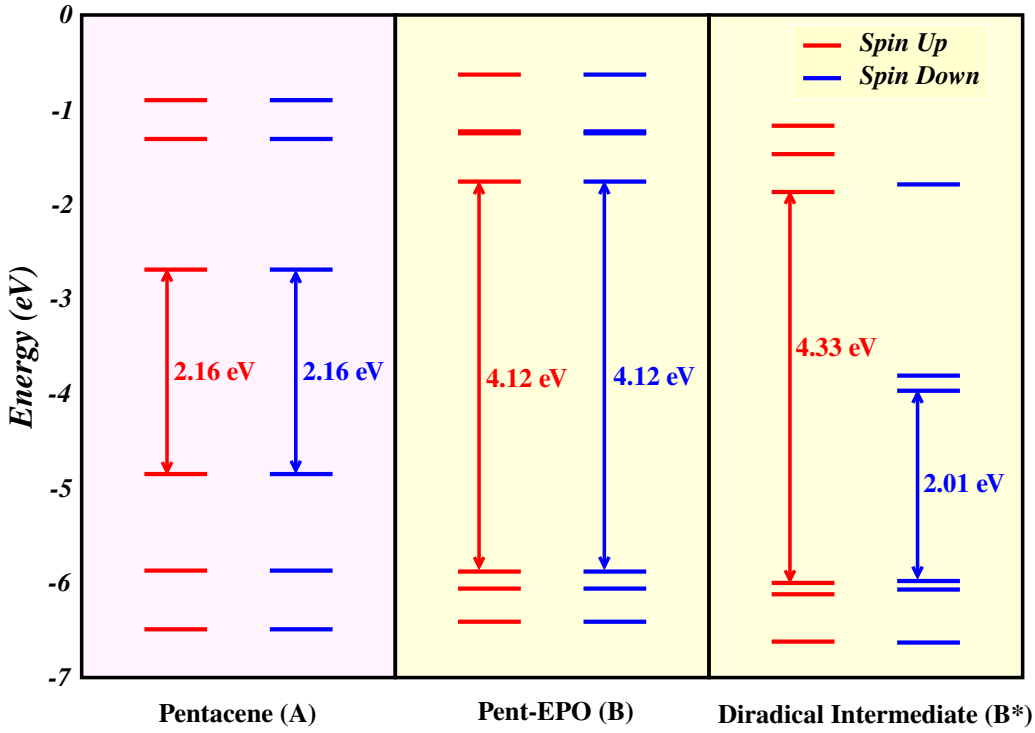

Figure S1: Frontier molecular orbital energies and HOMO-LUMO energy gaps computed at B3LYP/def2-TZVP level for pentacene (A), pent-EPO (B) and its diradical intermediate (B*). Red and blue color denotes spin up and spin down energy levels respectively. The different background pink and yellow colors denotes different degrees of conjugation, that is, fully conjugated for pentacene and broken conjugated for B and B*.

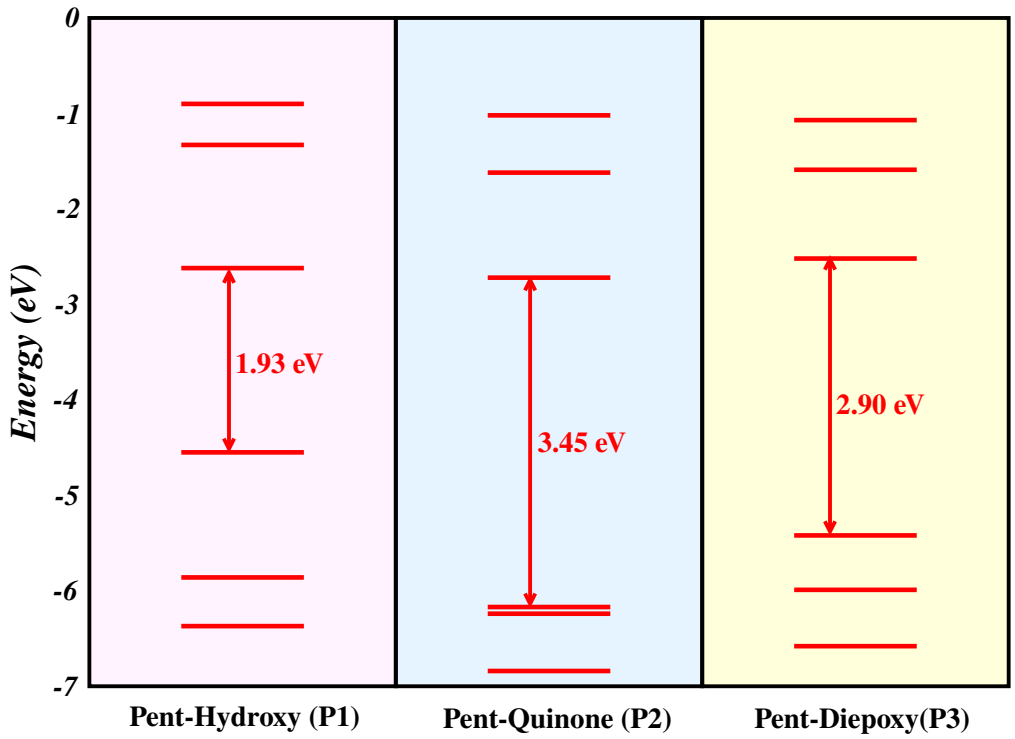

Figure S2: Frontier molecular orbital energies and HOMO-LUMO energy gaps computed at B3LYP/def2-TZVP level for photoproducts of pent-EPO including dihydroxypentacene (P1), pentaquinone (P2) and diepoxypentacene (P3). Due to spin degenerate levels, energy levels are shown for only one of the spin configuration. The background pink, blue and yellow colors represents the different degrees of conjugation, that is, fully conjugated, cross conjugated and broken conjugated respectively.

2 Molecular orbitals of isolated molecules

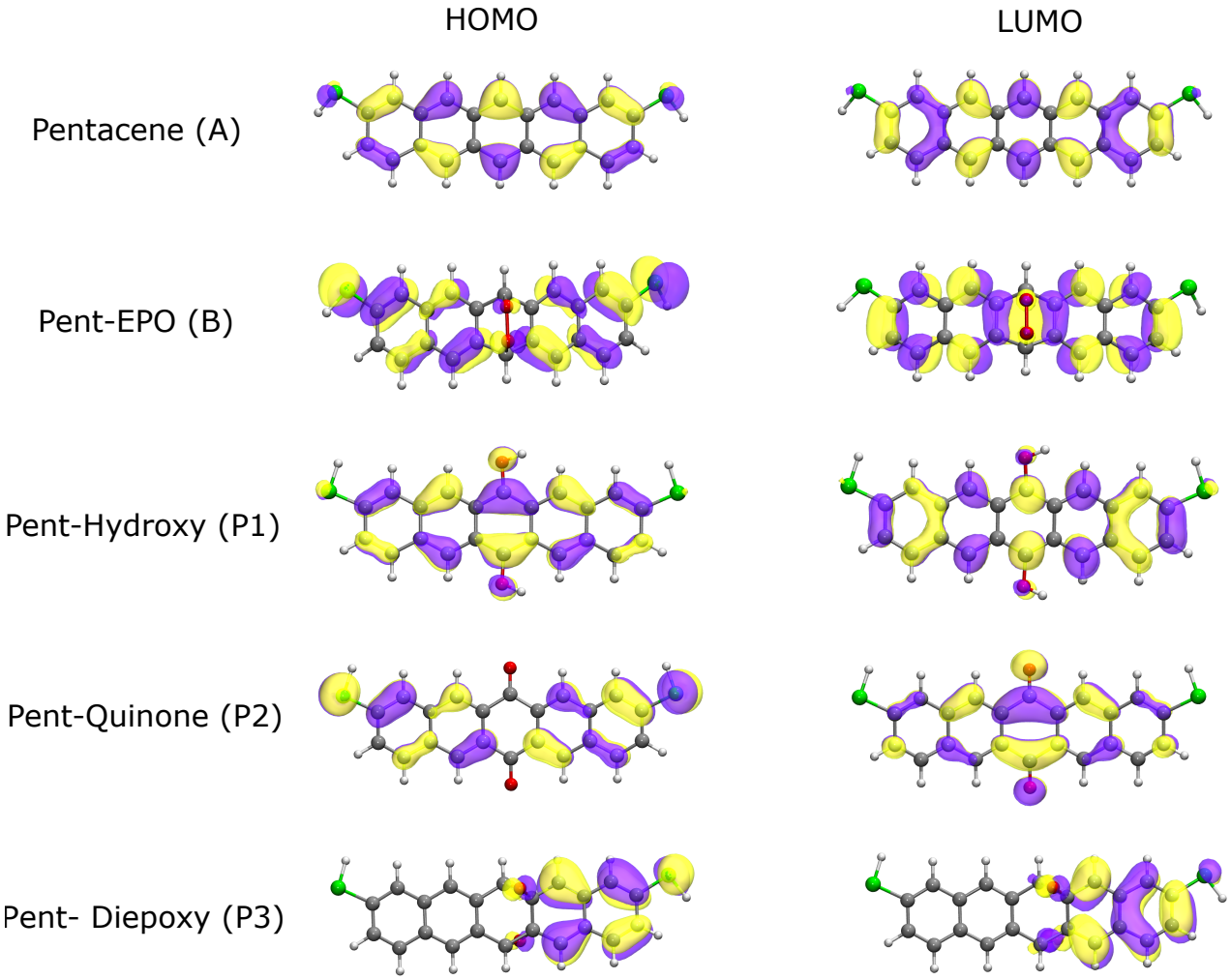

Figure S3: Spatial distribution of frontier HOMO and LUMO of pentacene (A), pent-EPO (B) and related photoproducts P1, P2 and P3 in isolated state computed using B3LYP/def2-TZVP method at an isovalue of 0.03.

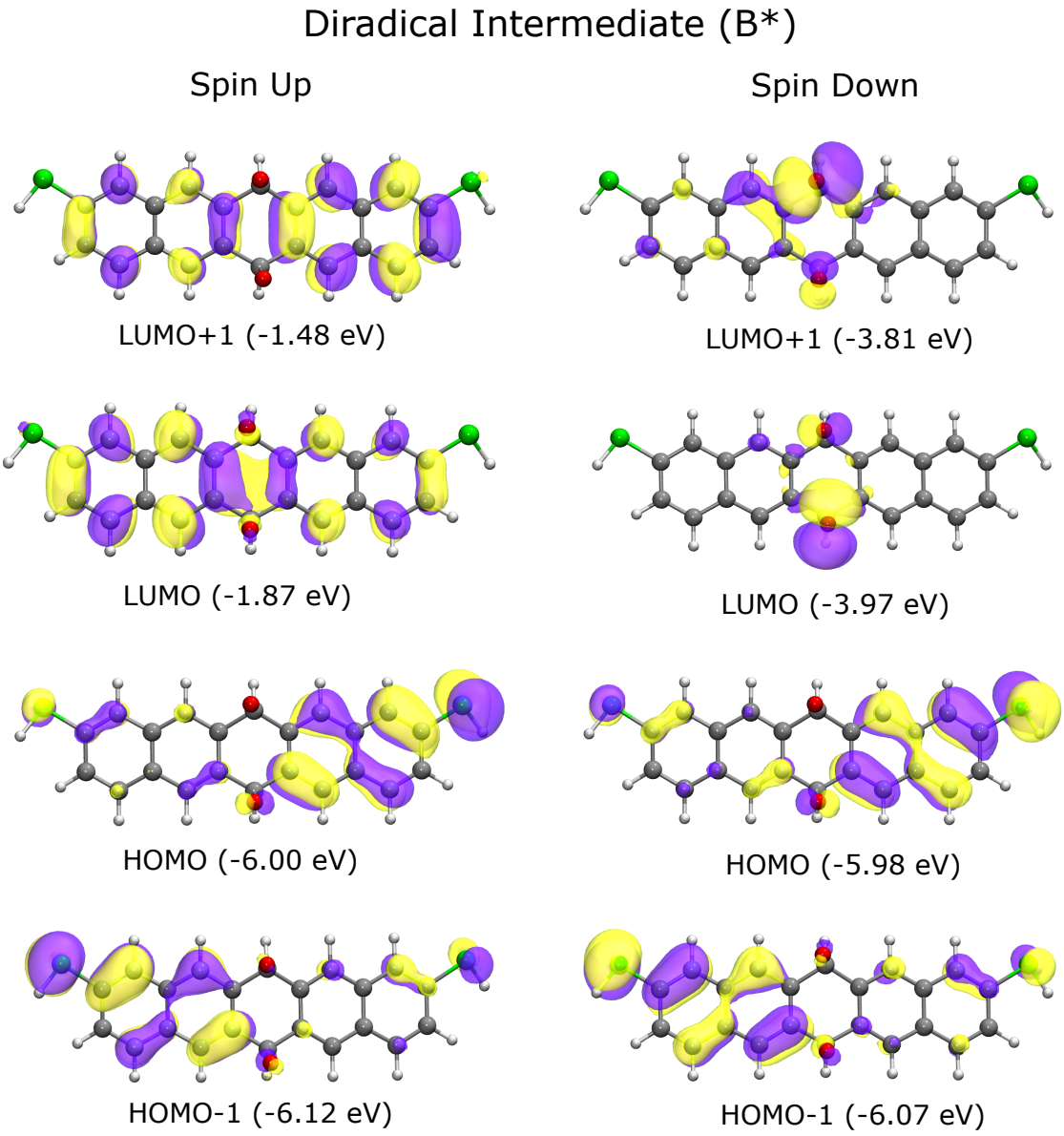

Figure S4: Spatial distribution of spin up and spin down frontier molecular orbitals of diradical intermediate of pent-EPO (B*) in isolated state computed using B3LYP/def2-TZVP method at an isovalue of 0.03.

3 Para connected diradical intermediate

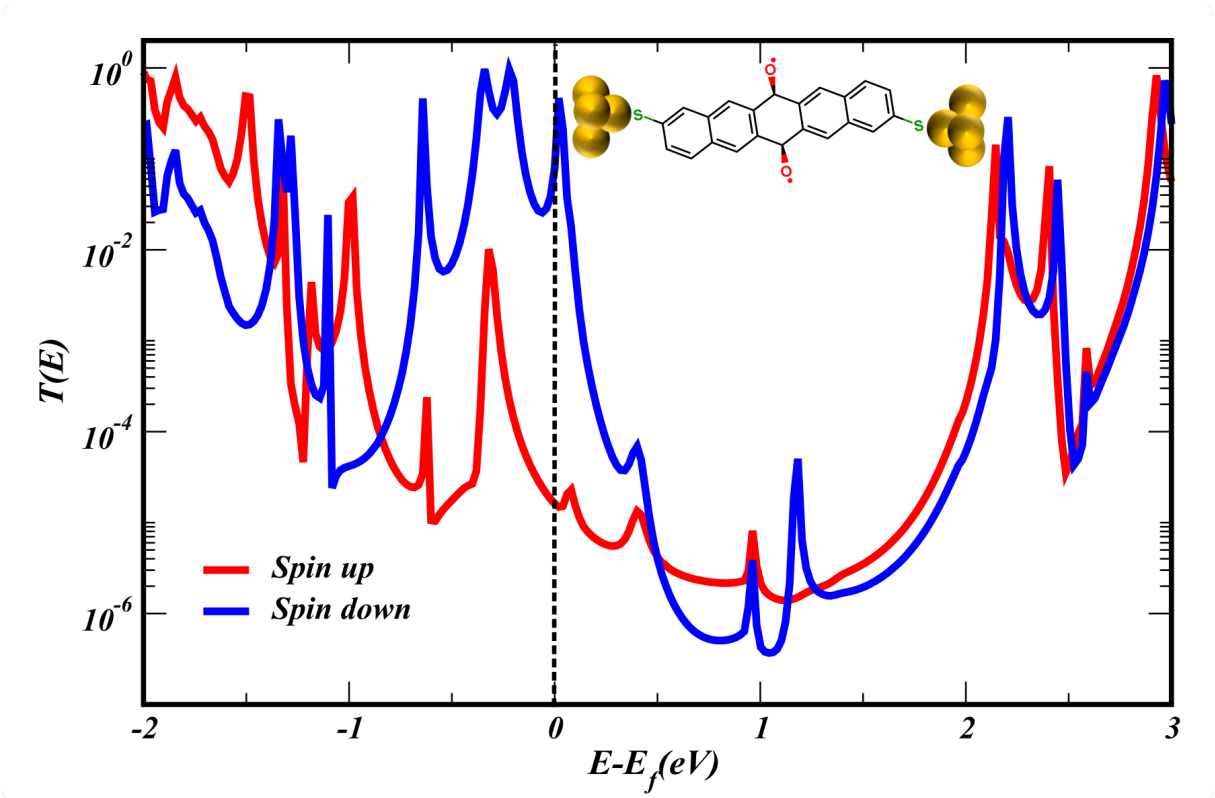

Figure S5: Spin resolved transmission spectra of diradical intermediate with para connection to gold electrodes. The spin up and spin down transmission is denoted by red and blue colors respectively. A high SFE of 99.0% is obtained for B* in para connection.

4 Broken conjugated Dihydropentacene

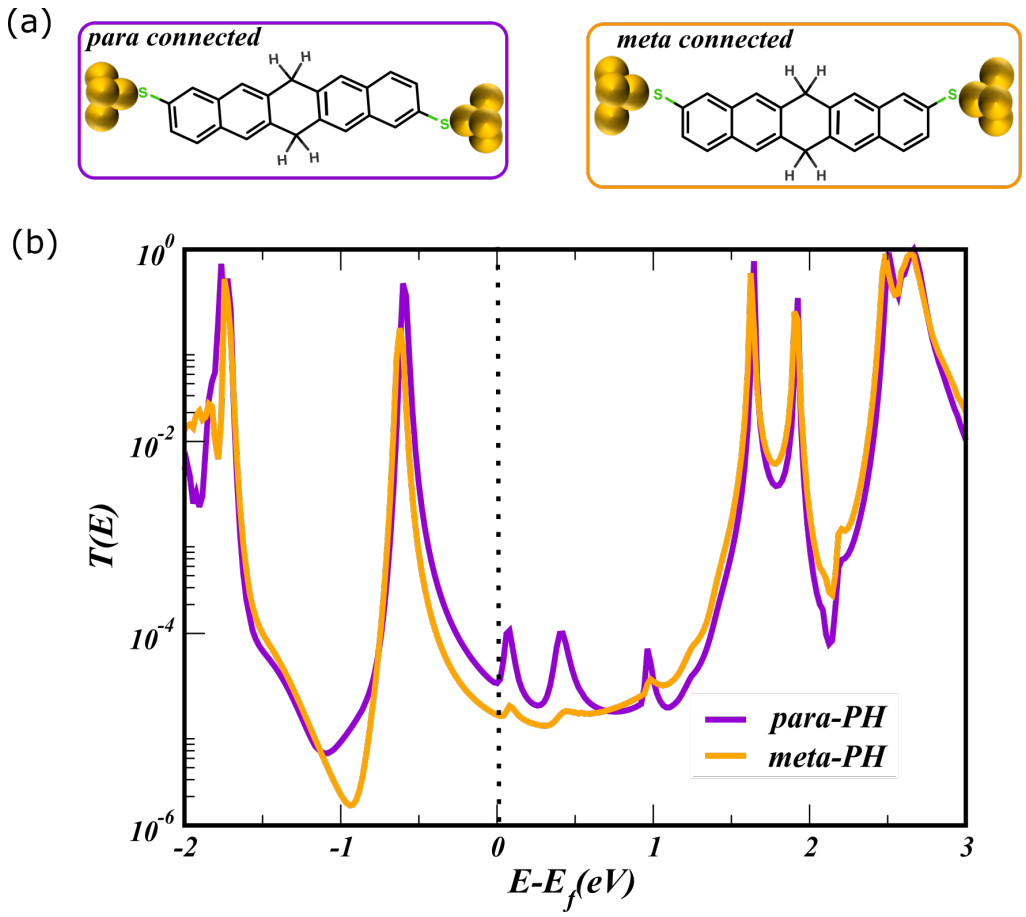

Figure S6: a) Dihydropentacene (PH) held between two Au electrodes illustrating para and meta connections in purple and orange enclosures respectively. b) Computed transmission spectra of para-PH and meta-PH shown by purple and orange curves respectively. The vertical dotted line denotes the position of Fermi level.

5 PDOS of Diradical Intermediate

The PDOS on to the 2p orbitals of individual O-atoms reveals that for B* in isolated state, the two degenerate peaks at $\sim$ 0.5 eV corresponds to the different O-atoms. While in molecular junction, the two dominant peaks at Fermi energy and at 1.16 eV, arising due to the lifting of degeneracy, shows the contribution of both O-atoms in both the peaks.

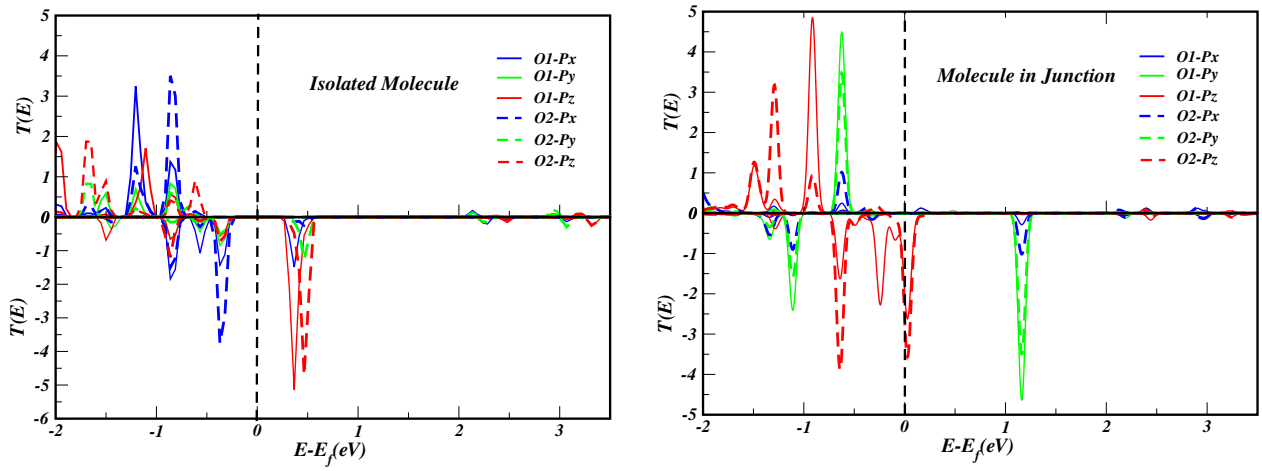

Figure S7: Projected density of states (PDOS) onto individual O(2p) atomic orbitals of diradical intermediate (B*) of EPO in isolated state (left panel) and in molecular junction (right panel). Solid lines indicates the PDOS on the 2p orbitals of first oxygen atom, while the dotted lines corresponds to second O-atom.

6 Transmission Eigenchannels

To gain additional insights in to the Quantum Interference (QI) perspectives, the transmission eigenchannels (EC) of molecular junctions are further investigated in both para and meta connections. In principle, the transmission eigenchannels coupled well with both left and right electrodes results in a fully conductive channel and yields higher conductance. While the weakly decaying channels exhibiting weak coupling with the terminal electrodes results in lower conductance. The transmission eigenchannels of parent pentacene shown in Fig. S8 illustrates that for *p*-Pent, both the left and right EC shows strong terminal coupling with electrodes. While for *m*-Pent both the ECs shows relatively weaker coupling with one of the terminating electrode. Thus, indicating lower conductance of *m*-Pent as compared to *p*-Pent.

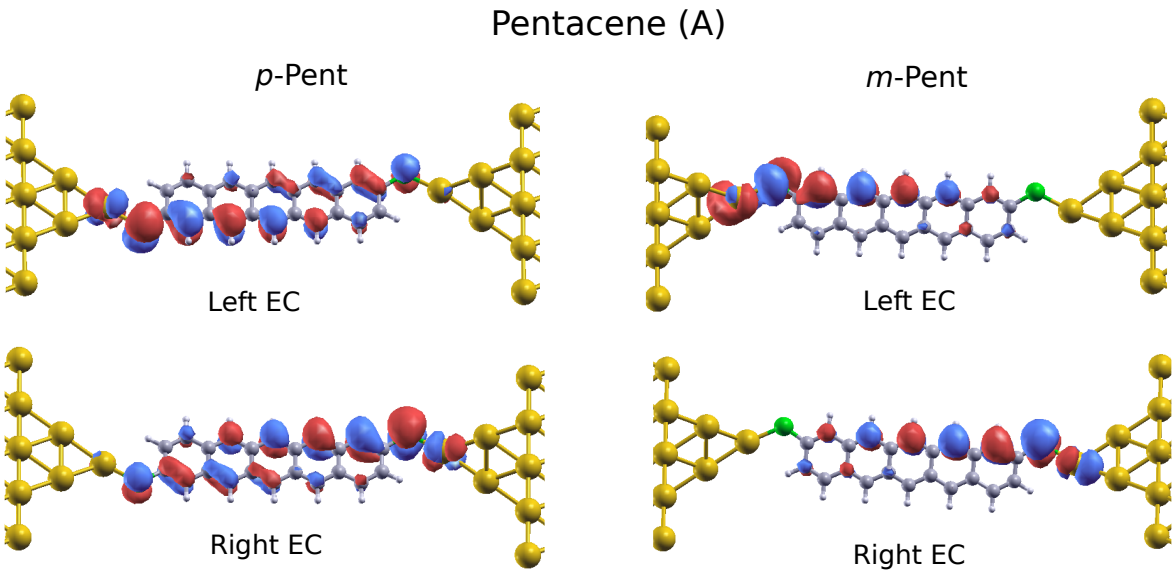

Figure S8: Transmission eigenchannels of p-Pent and m-Pent. m-Pent has weakly coupled channels.

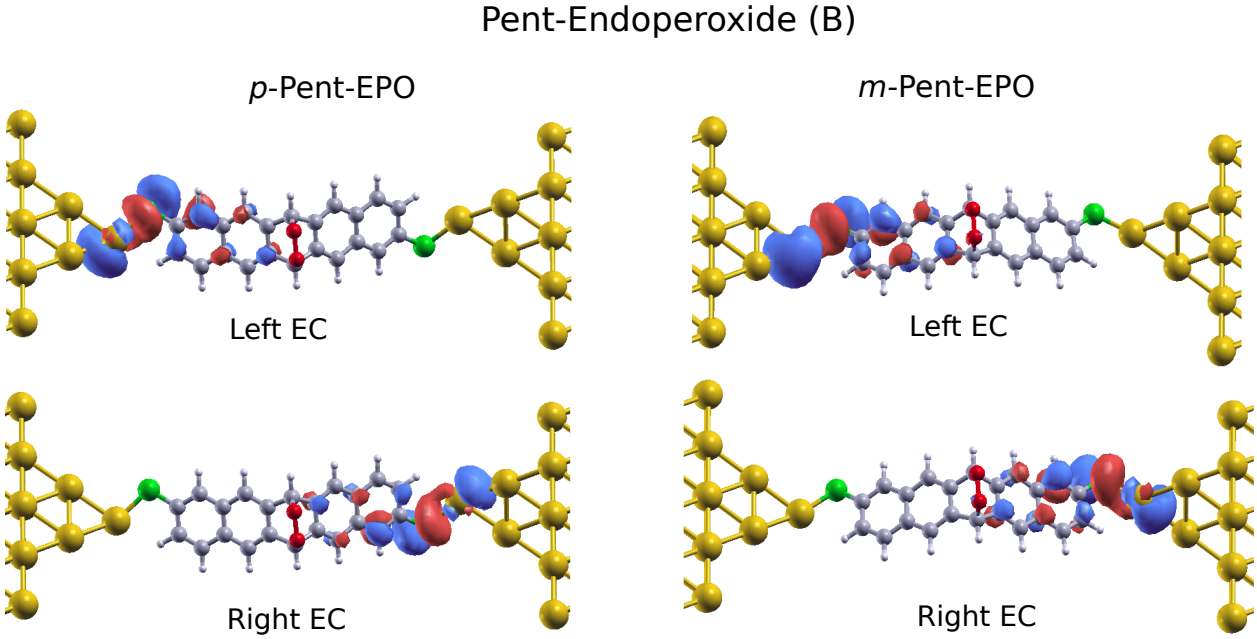

Figure S9: Transmission eigenchannels of p-Pent-EPO and m-Pent-EPO. ECs are identical for both para and meta connected pent-EPO.

For broken conjugated EPO, ECs of both p-Pent-EPO and m-Pent-EPO (shown in Fig. S9) are vanished on the peroxide bridge. Thus, indicating that the broken conjugation hinders the electron transport in both para and meta connections. Similarly, for diradical in-

termediate (B*), the spin up ECs are vanished on peroxide bridge. While spin down channels are fully conductive, however this behavior is identical for both para and meta connections. This strongly supports our observation that broken conjugation abandons the presence of QI features.

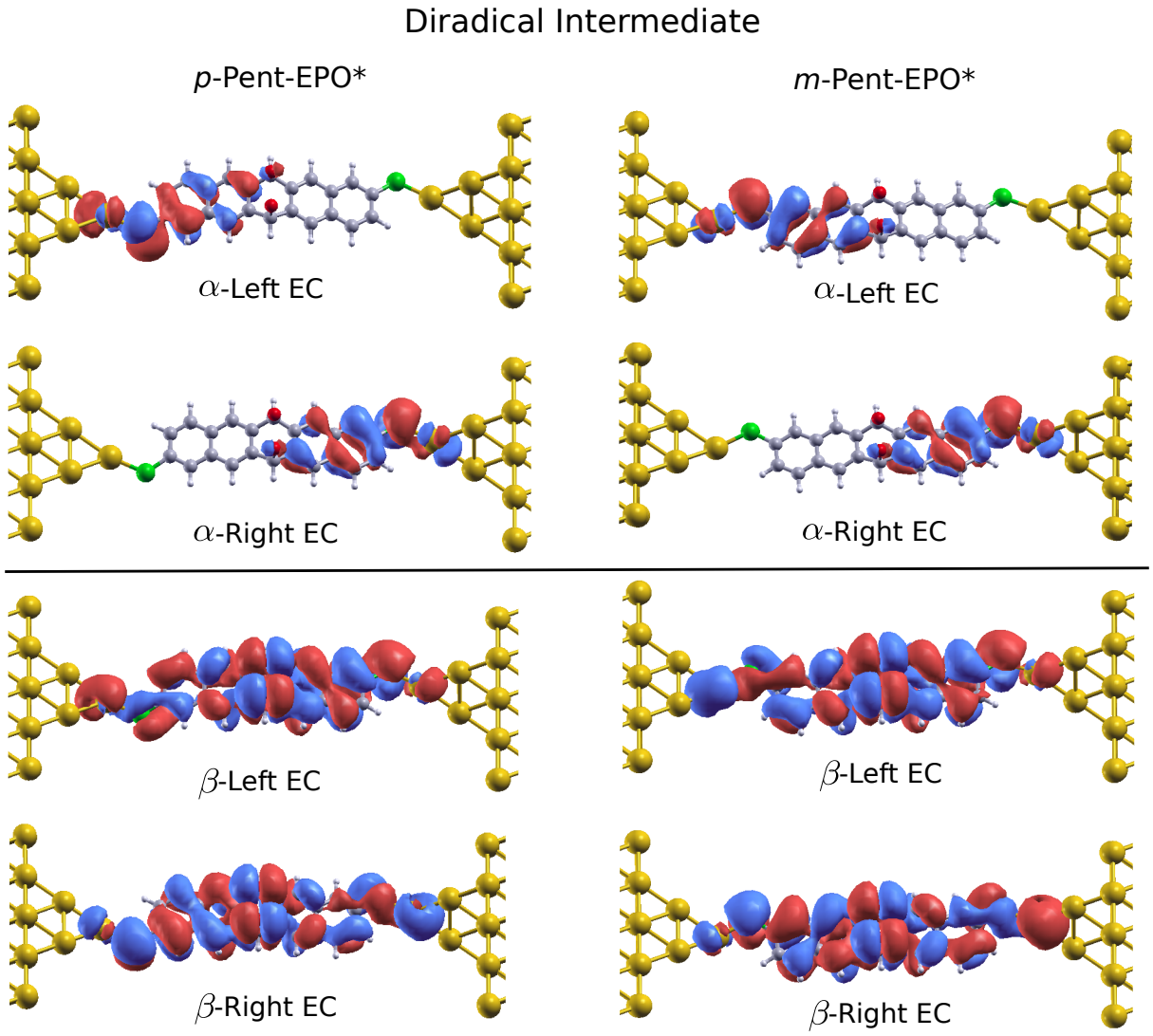

Figure S10: Transmission eigenchannels for spin up (top) and spin down (bottom) channels of diradical intermediate (B*). Spin down ECs are more conductive than spin up, but identical for both para and meta connections.

For photoproducts, the ECs of fully conjugated dihydroxypentacene (P1) reveals identical behavior as of pentacene. For Pentaquinone (P2), ECs of *m*-Pent-Quinone are coupled to both the electrodes, while for *p*-Pent-Quinone, ECs are relatively weakly coupled to

one of the electrode. This behaviour is in contrast to pentacene. For broken conjugated diepoxypentacene (P3), ECs are identical for both para and meta connections.

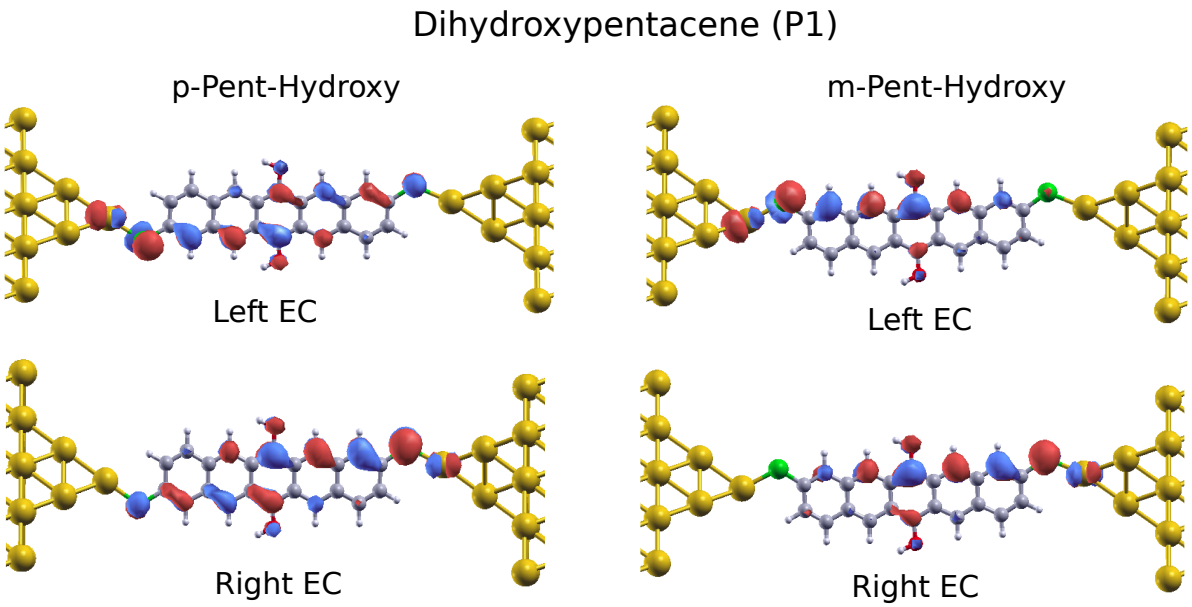

Figure S11: Transmission eigenchannels of P1; *p*-Pent-Hydroxy and *m*-Pent-Hydroxy. Terminal coupling is weaker for *m*-Pent-Hydroxy.

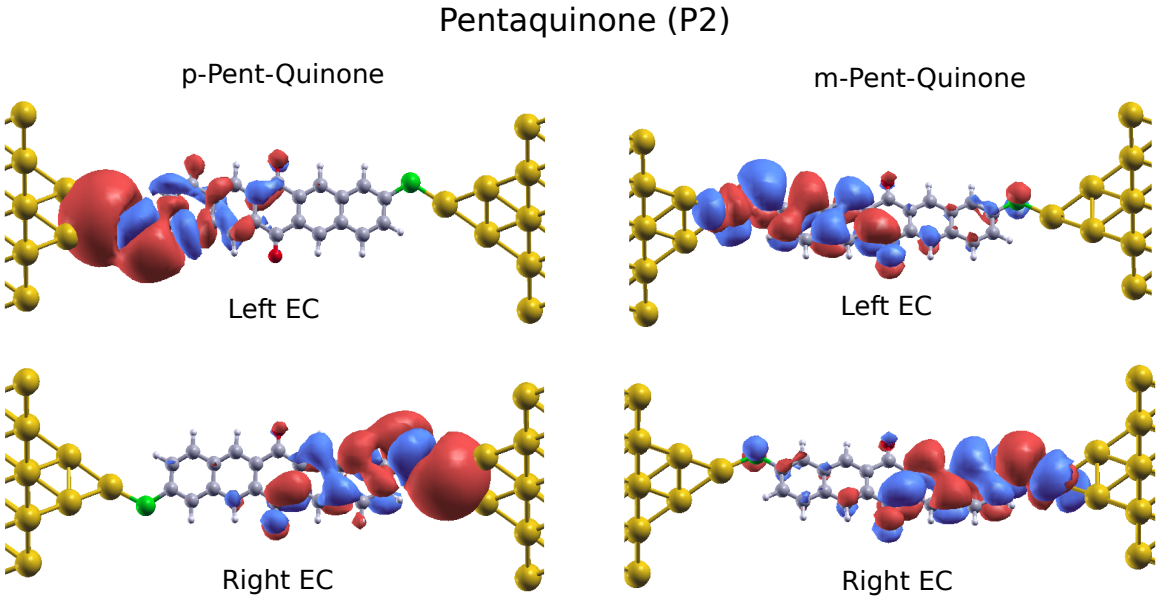

Figure S12: Transmission eigenchannels of P2; *p*-Pent-Quinone and *m*-Pent-Quinone. Terminal coupling is weaker for *p*-Pent-quinone.

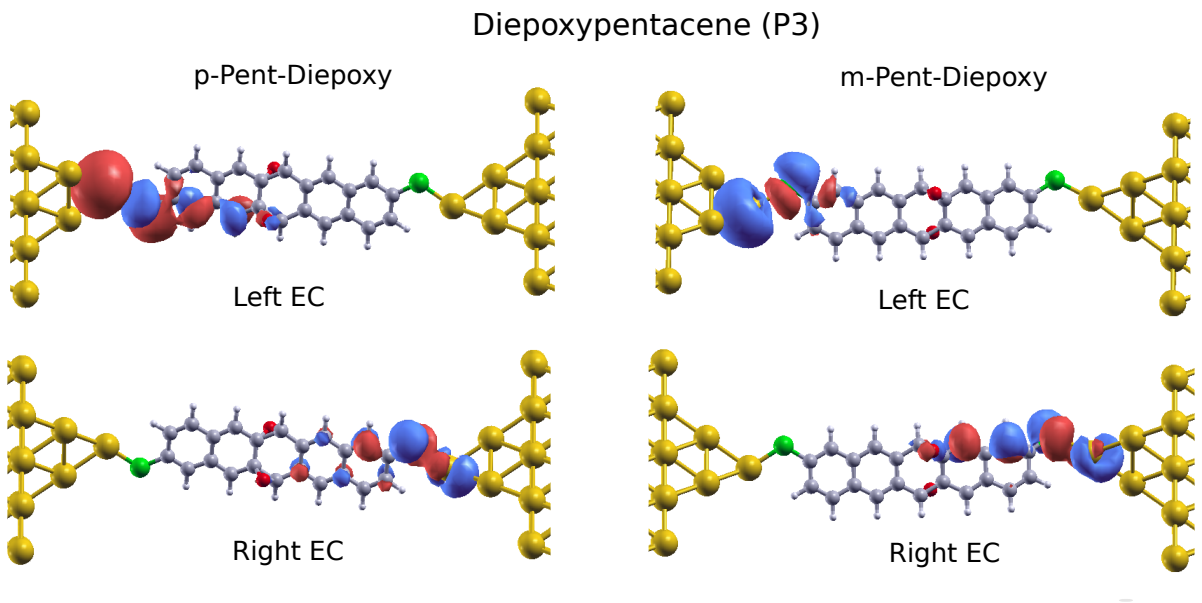

Figure S13: Transmission eigenchannels of P3; *p*-Pent-Diepoxy and *m*-Pent-Diepoxy. Both para and meta connection shows weak terminal coupling with one of the electrode.